analytical chemistry

pubs.acs.org/ac Article

Construction of a Dye-Sensitized and Gold Plasmon-Enhanced Cathodic Photoelectrochemical Biosensor for Methyltransferase Activity Assay

Lin Cui,[‖] Jingzhu Shen,[‖] Chen-Chen Li,[‖] Pei-Pei Cui, Xiliang Luo,* Xiaolei Wang,* and Chun-Yang Zhang*

Cite This: *Anal. Chem.* 2021, 93, 10310−10316 Read Online

ACCESS | Metrics & More | Article Recommendations | Supporting Information

ABSTRACT: DNA methyltransferases may function as important biomarkers of cancers and genetic diseases. Herein, we develop a dye-sensitized and gold plasmon-enhanced cathodic photoelectrochemical (PEC) biosensor on the basis of p-type covalent organic polymers (COPs) for the signal-on measurement of M.SssI methyltransferase (M.SssI MTase). The cathodic PEC biosensor is constructed by the *in situ* growth of p-type COP films onto a glass coated with indium tin oxide and the subsequent assembly of biotin- and HS-labeled double-stranded DNA (dsDNA) probes onto the COP film *via* biotin−streptavidin interaction. The dsDNA probe contains the recognition sequence of M.SssI MTase. The COP thin films possess a porous ultrathin nanosheet structure with abundant active sites, facilitating the generation of a high photocurrent compared with the hydrothermally synthesized ones. The presence of DNA methyltransferases can prevent the digestion of restriction endonuclease HpaII, consequently inducing the introduction of gold nanoparticles (AuNPs) to the dsDNA probes *via* the S−Au bond and the intercalation of rhodamine B (RhB) into the DNA grooves to produce a high photocurrent due to the dye-photosensitized enhancement and AuNP-mediated surface plasmon resonance. However, in the absence of M.SssI MTase, HpaII digests the dsDNA probes, and neither AuNPs nor RhB can be introduced onto the electrode surface, leading to a low photocurrent. This cathodic PEC biosensor possesses high sensitivity and good selectivity, and it can screen the inhibitors and detect M.SssI MTase in serum as well.

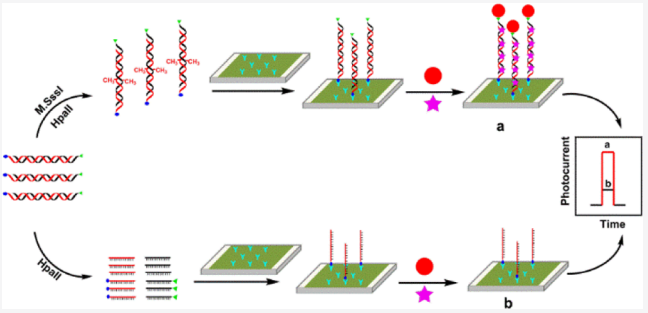

DNA methylation is a well-studied epigenetic modification,[1,2] and abnormal DNA methylation may cause various cancers (*e.g.*, thyroid tumor and breast cancer).[3−5] In eukaryotes, MTase catalyzes DNA methylation, and its aberrant activity may induce genetic diseases and cancers, and thus DNA MTase may act as an important biomarker. Until now, high-performance liquid chromatography,[6] fluorescent assay,[7] electrochemiluminescent assay,[8] polymerase chain reaction,[9] colorimetric assay,[10] and gel electrophoresis[11] have been developed to detect the MTase activity. However, they usually require expensive equipment, laborious sample treatment, and complex operation processes. New methods with the capability of simply and sensitively detecting MTase activity are highly required.

Photoelectrochemical (PEC) biosensors combine the merits of both optical and electrochemical biosensors,[12−19] and they have totally separated optical excitation and signal readouts, with distinct advantages of easy operation, fast response, low cost, and low background.[20] Their signaling mechanism mainly relies on the alteration of electron donor/acceptor concentration or the change of diffusion efficiency for the achievement of signal diminution/enhancement,[21,22] and the drop-coating modification method is frequently employed to construct the electrodes of PEC biosensors.[23,24] However, the instability and unrepeatability of photoactive materials may disturb the charge mobility on the electrode and adversely influence the sensing performance. Generally, PEC sensing relies on photoresponsive materials. n-Type semiconductors (*e.g.*, Bi_2S_3, CdS, TiO_2, and ZnO) have been extensively employed for the development of PEC sensors.[25,26] However, the n-type semiconductors as photoanodes are easily interfered by the reaction of strongly reducing substances and oxidizing holes. p-Type semiconductors can function as photocathodes, and they interact with electron acceptors instead of electron donors, efficiently resisting the reductive agents[27] and photocorrosion.[28] Recently, the p-type semiconductors have

Received: April 27, 2021
Accepted: July 7, 2021
Published: July 14, 2021

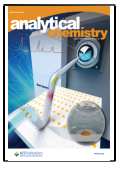

https://doi.org/10.1021/acs.analchem.1c01797
Anal. Chem. 2021, 93, 10310−10316

Scheme 1. (A) *In Situ* Synthesis of a Porous COP onto an ITO Glass Substrate and (B) Development of a PEC Biosensor for M.SssI MTase Assay

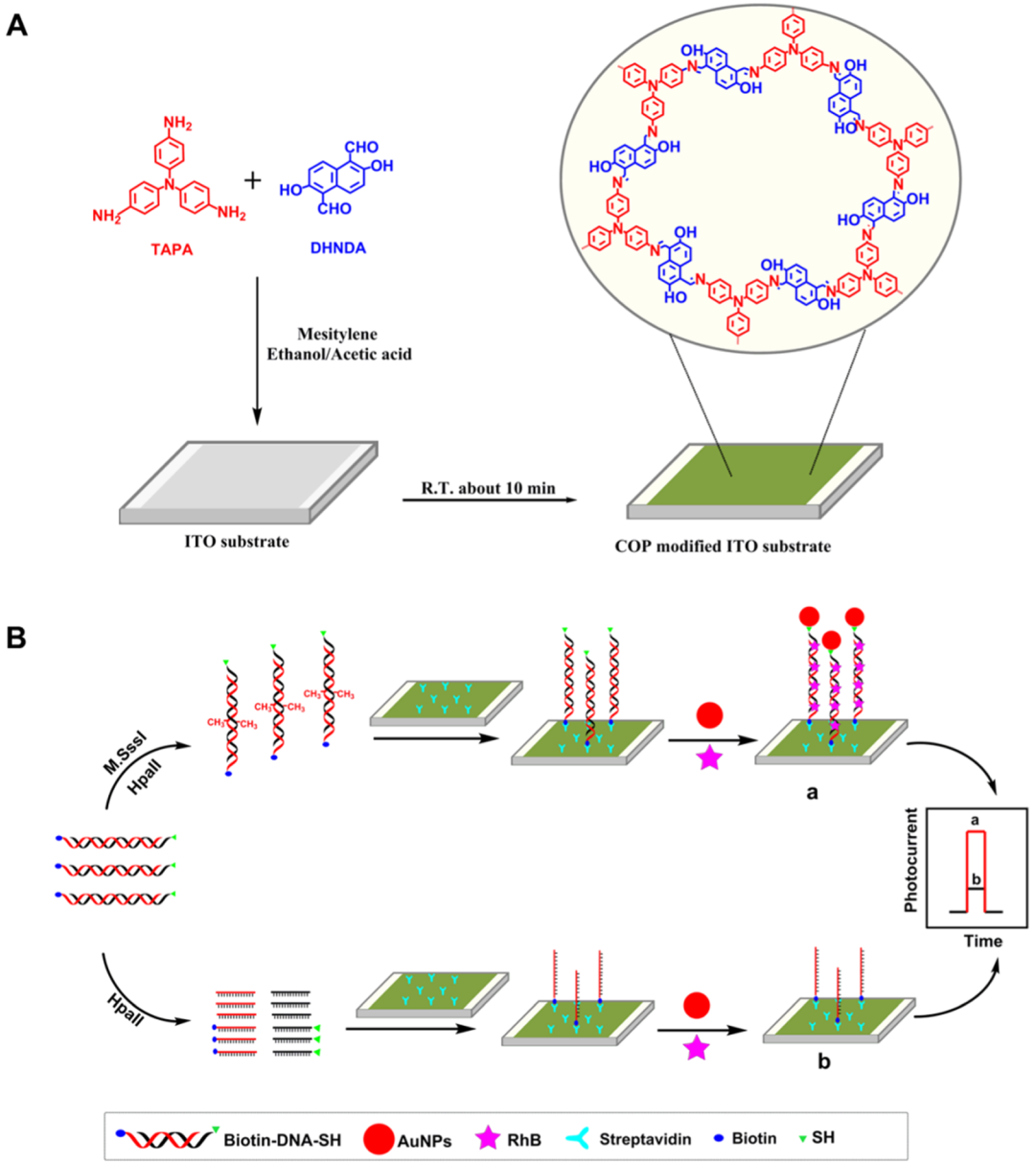

attracted more and more attention in the development of cathodic PEC sensors.[29−32] Polymer compounds such as triazine−thiadiazole-based copolymers,[33] arylacetylene-based copolymers,[34] and polythiophene[35] exhibit p-type semiconductor properties, with promising applications in energy conversion and active photocathodes.[36] Covalent organic polymers (COPs) are porous polymer compounds with the characteristics of large specific surface area, good stability, adjustable function, and controllable structure[37] and have been widely applied in drug delivery,[38,39] catalysis,[40] gas storage/separation,[41−43] sensing,[44] and energy storage.[50] Especially, the strong $\pi-\pi$ stacking between two-dimensional COP layers can produce high porosity and crystallinity, providing a transport channel for carrier transformation and consequently making COPs become excellent photoactive materials for PEC biosensors.

Noble-metal nanoparticles exhibit surface plasmon resonance (SPR),[46,47] with the characteristics of visible light-induced charge separation, intensive localized electric field, and the unique plasmon absorbance.[48−50] Gold nanoparticles (AuNPs) have the advantages of controlled synthesis, good stability, biocompatibility, and catalytic performance.[51] Especially, the SPR of AuNPs can enhance the photocurrent-transfer efficiency. Herein, we develop a dye-sensitized and gold plasmon-enhanced cathodic PEC biosensor based on p-type COP thin films for the signal-on measurement of M.SssI MTase. The cathodic PEC biosensor is constructed by the *in situ* growth of p-type COP films onto an indium tin oxide (ITO)-coated glass and the subsequent assembly of biotin- and HS-labeled double-stranded DNA (dsDNA) probes with the M.SssI MTase recognition sequence onto the COP films. The presence of DNA methyltransferases can prevent the digestion of restriction endonuclease HpaII, consequently inducing the introduction of AuNPs to the dsDNA probes *via* the S−Au bond and the intercalation of rhodamine B (RhB) into the DNA grooves to produce a high photocurrent. The SPR effect

https://doi.org/10.1021/acs.analchem.1c01797
Anal. Chem. 2021, 93, 10310−10316

of AuNPs and the RhB photosensitive enhancement can significantly amplify the photocurrent of the PEC biosensor. This cathodic PEC biosensor can screen the inhibitors and detect M.SssI MTase in serum as well.

EXPERIMENTAL SECTION

General. The reagents and materials as well as the apparatus and characterization are described in the Supporting Information

***In Situ* Synthesis of COP onto ITO.** Prior to use, the ITO slices (4.7 cm × 1 cm) were sonicated in acetone, 10% H_2O_2, and 1.0 M NaOH, followed by ultrapure water cleaning and nitrogen blow-drying. 4,4′,4″-Triaminotriphenylamine (TAPA, 1 mg) and 2,6-dihydroxynaphthalene-1,5-diformaldehyde (DHNDA, 1 mg) were dissolved in 550 μL of a solution containing acetic acid, mesitylene, and ethanol (v/v/v = 1:5:5), respectively, followed by mixing together (v/v = 1:1) and dripping 20 μL of the mixture solution onto ITO at room temperature. After 10 min, the unreacted residues were removed from the ITO glass by using methylene chloride. A thin rosybrown-colored film was obtained on the ITO surface after drying at room temperature (Figure S1, middle).

Construction of the PEC Biosensor. The PEC biosensor was constructed by creating a hollow-carved circle with a diameter of 0.4 cm (surrounded by an insulation tape) in the COP film-modified ITO electrode (Figure S1, right). The streptavidin/COP/ITO electrode was obtained by sequentially dropping 20 μL of streptavidin solution (0.1 mM) onto the COP/ITO electrode and subsequently drying at room temperature.

Detection of M.SssI MTase Activity and Inhibition Assay. To reduce the disulfide-bonded oligonucleotides, TCEP was used to activate DNA-1 probes for 1 h. The 2 μM DNA-1 hybridized with 2 μM DNA-2 in the buffer (5 mM $MgCl_2$, 1.0 mM ethylenediaminetetraacetic acid, and 10 mM Tris, pH 7.4) at 37 °C for 30 min to obtain the dsDNA probes. Then, 15 μL of the dsDNA probes (2 μM) was incubated with 2.0 μL of 1× NEBuffer 2, M.SssI MTase, and 160 μM SAM at 37 °C for 2 h, followed by incubation with 100 U mL^{-1} HpaII + 1× CutSmart buffer at 37 °C for 2 h. The AuNPs/dsDNA/streptavidin/COP/ITO electrode was obtained by dripping the reaction solution onto the streptavidin/COP/ITO electrode, incubating for 30 min, washing with 0.1 M PBS, and incubating with AuNPs (20 μL) for 8 h. After incubating the modified electrode with 1 mM RhB for 30 min and subsequent washing with 0.1 M PBS, the PEC measurements were performed in 0.1 M PBS. Inhibition assay was carried out by incubating inhibitors of different concentrations with 100 U mL^{-1} M.SssI MTase, followed by the measurement procedures described above.

RESULTS AND DISCUSSION

Principle of M.SssI MTase Detection. The imine condensation reaction was performed at room temperature for the *in situ* synthesis of COP films onto ITO, with TAPA and DHNDA as the building blocks (Scheme 1A). The PEC biosensor was constructed by the subsequent assembly of biotin- and HS-labeled dsDNA probes containing the M.SssI MTase recognition sequence onto the COP film *via* the biotin–streptavidin interaction (Scheme 1B). The dsDNA probe was constructed with two complementary single-stranded DNA strands which contain the CpG dinucleotide site 5′-CCGG-3′, with DNA-1 being labeled by thiol and DNA-2 being labeled by biotin at the 3′ end. The presence of M.SssI MTase enables the methylation of 5′-CCGG-3′ which prevents the recognition of HpaII, and thus dsDNAs remained on the COP/ITO electrode. Subsequently, AuNPs are assembled onto the dsDNA/COP/ITO photocathode through the S–Au interaction, and RhB is inserted into the dsDNA groove. The SPR effect and excellent conductivity of AuNPs coupled with the RhB photosensitive enhancement can significantly amplify the cathodic photocurrent. In the absence of M.SssI MTase, the methylation of 5′-CCGG-3′ cannot occur, and HpaII can digest the dsDNA probes. Consequently, neither AuNPs nor RhB can be immobilized onto the electrode, and no enhanced cathodic photocurrent is detected.

Characterization of the COP Film and the AuNPs. The synthesis of the COP thin film is confirmed by the Fourier transform infrared (FT-IR) spectrum. The FT-IR spectrum of DHNDA (Figure 1A, blue line) exhibits a C–H stretching

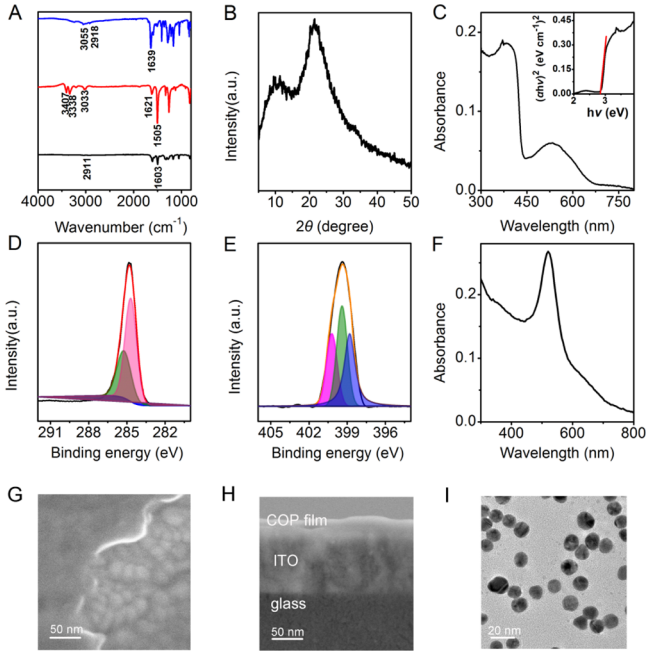

Figure 1. (A) FT-IR spectra of TAPA (red), DHNDA (blue), and the COP film (black). (B,C) XRD data (B) and diffuse reflectance spectrum (C) of the COP film. Inset of (C) shows the Tauc plot. (D,E) High-resolution XPS spectra of C 1s (D) and N 1s (E) of the COP film. (F) UV–vis spectrum of the AuNPs. (G,H) SEM top view (G) and cross section (H) of the COP film onto ITO. (I) TEM image of the AuNPs.

vibration (2918 cm^{-1}) and a carbonyl group stretching vibration (1639 cm^{-1}).[52] The FT-IR spectrum of TAPA (Figure 1A, red line) shows stretching frequencies of 3338 cm^{-1} (N–H of amine ring) and 1621 cm^{-1} (C=C of phenyl). After the condensation of monomers (Figure 1A, black line), the characteristic N–H stretching band of TAPA (3338 cm^{-1}) and the C=O stretching band of DHNDA (1639 cm^{-1}) disappear, and a new C–H stretching frequency of phenyl ring (2911 cm^{-1}) and a new C=N stretching band (1603 cm^{-1}) appear, verifying the formation of COP from DHNDA and TAPA (Figure 1A, black line).[45] XRD is further used to characterize the COP thin film (Figure 1B). Two broad peaks at 21.8 and 11.5° correspond to the [001] and [100] planes,

https://doi.org/10.1021/acs.analchem.1c01797
Anal. Chem. 2021, 93, 10310–10316

respectively, with the [001] plane being induced by the $\pi-\pi$ stacking between the COP layers. UV−vis diffuse reflectance spectroscopy shows that the COP thin film possesses a 300−600 nm absorption band with a tail of more than 700 nm (Figure 1C). The COP band gap (E_g) of 2.89 eV is obtained based on eq 1[53]

$$\alpha h\nu = A(h\nu - E_g)^{1/2} \quad (1)$$

where h is the Planck constant, α is the absorption coefficient, A is a constant term, ν is the frequency of light, and E_g is the band gap. Moreover, the C═N bond at 285.7 and 398.8 eV is detected in the high-resolution X-ray photoelectron spectroscopy (XPS) spectra of C 1s (Figure 1D) and N 1s (Figure 1E), respectively, further verifying the existence of imine linkers in the COP film. The UV−vis absorption spectrum displays that the 13 nm AuNPs show an absorption peak at 520 nm (Figure 1F). The scanning electron microscopy (SEM) image shows the assembly of a homogeneous and continuous COP film onto ITO (Figure 1G), with the boundary being hardly distinguished between the COP film and ITO (Figure 1H), suggesting the strong adherence of the ultrathin film onto ITO. The transmission electron microscopy (TEM) image indicates that AuNPs have a uniform size distribution with 13 nm diameter (Figure 1I).

Mechanism of PEC Biosensors. We compared the photocurrents of different modified ITO electrodes. The COP film-modified ITO electrode generates a higher photocurrent (−819 nA) than the bulk COP-modified ITO electrode constructed by the hydrothermal method (−95 nA) (Figure S2). Figure 2 shows that the photocurrent

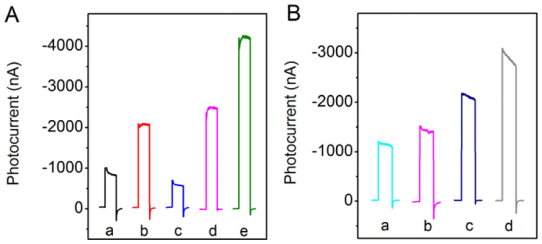

Figure 2. (A) Photocurrent generated by the COP/ITO electrode (a) and the AuNPs/COP/ITO electrode (b) in 0.1 M PBS, the AuNPs/COP/ITO electrode in deaerated electrolyte (c), the COP/ITO electrode (d), and the AuNPs/COP/ITO electrode (e) in 0.1 μM RhB + 0.1 M PBS. (B) Photocurrent generated by the dsDNA/streptavidin/COP/ITO electrode in response to HpaII + AuNPs (a), HpaII + AuNPs + RhB (b), HpaII + M.SssI MTase + AuNPs (c), and HpaII + M.SssI MTase + AuNPs + RhB (d). 100 U mL^{-1} HpaII, 0.1 mM RhB, and 100 U mL^{-1} M.SssI MTase were used in the experiments.

generated by the AuNPs/COP/ITO electrode (−2073 nA, Figure 2A, curve b) is much higher than that generated by the COP/ITO electrode (−819 nA, Figure 2A, curve a). The following two factors make contributions to the enhanced cathodic photocurrent: (1) the direct contact between the AuNPs and the COP film facilitates charge transfer between them, and (2) the SPR effect of AuNPs enhances the separation efficiency of the photogenerated carriers. Notably, when the measurement is performed in a nitrogen-purging deaerated electrolyte, a lower photocurrent is detected (Figure 2A, curve c), suggesting the key role of oxygen as an electron acceptor in the cathodic photocurrent generation. The COP/ITO electrode generates a lower photocurrent (−2512 nA, Figure 2A, curve d) than the AuNPs/COP/ITO electrode (−4201 nA, Figure 2A, curve e) in 0.1 μM RhB + 0.1 M PBS, suggesting the high photocurrent induced by RhB photosensitive enhancement.

We further investigated the PEC behavior of the proposed biosensor (Figure 2B). The dsDNA/streptavidin/COP/ITO electrode generates a higher photocurrent in response to HpaII + M.SssI MTase + AuNPs (−2048 nA, Figure 2B, curve c) than that in response to HpaII + AuNPs (−1120 nA, Figure 2B, curve a), suggesting the feasibility of this biosensor for M.SssI MTase detection. Notably, the dsDNA/streptavidin/COP/ITO electrode generates a higher photocurrent in response to HpaII + M.SssI MTase + AuNPs + RhB (−2738 nA, Figure 2B, curve d) than those in response to HpaII + AuNPs + RhB (−1416 nA, Figure 2B, curve b) and HpaII + M.SssI MTase + AuNPs (−2048 nA, Figure 2B, curve c), suggesting the enhanced photocurrent induced by the intercalation of dye-sensitized RhB in the DNA grooves.

Scheme 2 illustrates the mechanism of light irradiation-induced photocurrent from the COP film in the PEC

Scheme 2. Mechanism of Light Irradiation-Induced Photocurrent from the COP Film in the PEC Biosensor[a]

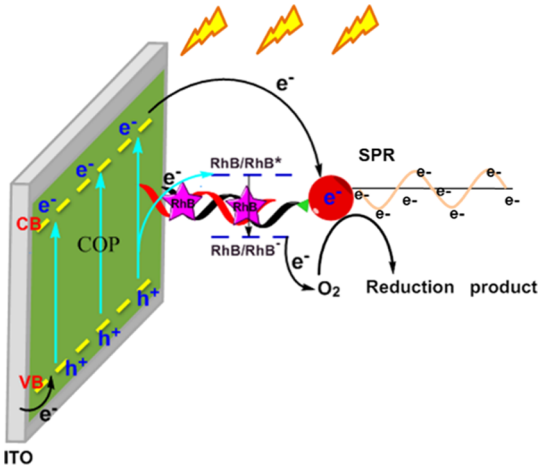

[a]CB, conduction band; VB, valence band.

biosensor. Under light irradiation, photoexcitation of the COP film induces the electron transfer from the valence band (VB) to the conduction band (CB), generating electron−hole pairs. Then, the excited electrons on the CB of the COP film quickly inject into the AuNPs due to the AuNP-mediated SPR effect, enhancing the carrier separation efficiency. Subsequently, the dissolved oxygen can react with the electrons on the CB of the AuNP surface and the COP film to generate a high cathodic photocurrent.[49] Meanwhile, RhB can harvest visible light to form RhB*, and the electron can transfer from the VB of the COP film to the excited-state RhB* (eq 2).[54] Subsequently, an electron transfers from the reduced dye RhB$^-$ (eq 3) to O_2, regenerating RhB and forming a reduction product of O_2 (eq 4). In addition, the excellent conductivity and SPR effect of AuNPs coupled with RhB photosensitive enhancement facilitate the electron transfer and the generation of an enhanced photocurrent.[55]

$$\text{RhB/COP} + h\nu \rightarrow \text{RhB*/COP (excitation)} \quad (2)$$

https://doi.org/10.1021/acs.analchem.1c01797
Anal. Chem. 2021, 93, 10310−10316

$$RhB^*/COP \rightarrow RhB^-/COP(h^+)\ (\text{hole injection}) \quad (3)$$

$$RhB^-/COP(h^+) + O_2 \rightarrow RhB/COP(h^+) + \text{reduction product of } O_2\ (\text{dye regeneration and } O_2 \text{ reduction}) \quad (4)$$

Sensitivity of M.SssI MTase Assay. We investigated the sensitivity of this biosensor under optimized conditions (Figure S3). M.SssI MTase generates concentration-dependent photocurrent (Figure 3A), and the photocurrent shows a linear

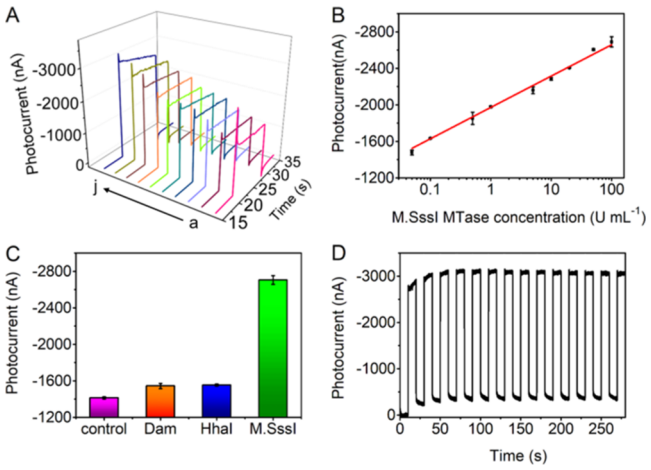

Figure 3. (A) Photocurrent generated by different concentrations of M.SssI MTase. The M.SssI MTase concentration is 0, 0.05, 0.1, 0.5, 1, 5, 10, 20, 50, and 100 U mL^{-1} from a to j. (B) A linear correlation is obtained between the photocurrent and the logarithm of the M.SssI MTase concentration. (C) Photocurrent generated by 100 U mL^{-1} Dam MTase (orange), 100 U mL^{-1} M.SssI MTase (green), 100 U mL^{-1} HhaI MTase (blue), and the control without any MTase (rose red). Error bars are the standard deviations of three independent experiments. (D) 14 cycles of continuous scanning for the assessment of the stability of the PEC biosensor.

correlation with the logarithm of the M.SssI MTase concentration in the range from 0.05 to 100 U mL^{-1}, with the corresponding equation being $I = -1951 - 362.4 \lg C$ ($R^2 = 0.9964$), where C is the concentration of M.SssI MTase (U mL^{-1}) and I is the measured photocurrent (Figure 3B). The detection limit is measured to be 0.022 U mL^{-1}, which is superior to those of previous biosensors (Table S1). The following factors make contributions to the high sensitivity of this PEC biosensor: (1) the function of the COP film as the electron donor facilitates the production of an enhanced photocurrent, (2) AuNPs with SPR effect and excellent conductivity can improve the photocurrent efficiency of the PEC biosensor, and (3) RhB harvests light, facilitating the electron transfer to the excited-state RhB* from the VB of COP for the achievement of an enhanced photocurrent.

Selectivity, Stability, and Reproducibility of the PEC Biosensor. We investigated the selectivity of this biosensor using HhaI MTase and DNA adenine MTase (Dam) as the interference enzymes (Figure 3C). Hhal MTase and Dam MTase cannot recognize and methylate the specific sequence 5′-GmCGCGC-3′ in the dsDNA probe used in this research. As a result, the photocurrents generated by Dam (−1544 nA) and HhaI MTase (−1554 nA) are much lower than that generated by M.SssI MTase (−2704 nA), suggesting the good selectivity of this PEC biosensor toward M.SssI MTase.

We further investigated the stability of this biosensor by performing 14 consecutive cycles of scans with light on and off (Figure 3D). The photocurrent generated by 100 U mL^{-1} M.SssI MTase remains unchanged for each on/off period, and the relative standard deviation (RSD) is measured to be 1.23%. To assess the reproducibility of this biosensor, we fabricated six electrodes under identical conditions and used them to detect 100 U mL^{-1} M.SssI MTase, respectively. The RSD is measured to be 0.21%, suggesting the excellent reproducibility of this biosensor.

Inhibition Assay. 5-Aza-2′-deoxycytidine (5-Aza-dC) and 5-azacytosine (5-Aza) are the inhibitors of M.SssI MTase. The relative activity of M.SssI MTase (RA) is measured based on eq 5

$$RA = \frac{C_i}{C_t} \times 100\% = 10^{(I_t - I_i)/362.4} \times 100\% \quad (5)$$

where I_t is the photocurrent generated by M.SssI MTase, and I_i is the photocurrent generated by M.SssI MTase + either 5-Aza (Figure 4A) or 5-Aza-dC (Figure 4B). C_t and C_i were obtained according to the linear correlation equation in Figure 3B, respectively.

$$I_t = -1951 - 362.4 \lg C_t \quad (6)$$

$$I_i = -1951 - 362.4 \lg C_i \quad (7)$$

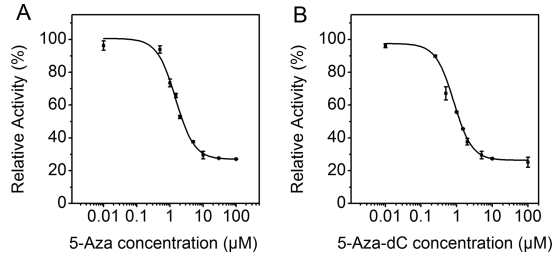

Figure 4. 5-Aza (A) and 5-Aza-dC (B) induce the concentration-dependent decrease of the relative activity of M.SssI MTase.

5-Aza induces the concentration-dependent decrease of relative activity of M.SssI MTase (Figure 4A), with the measured half-maximal inhibitory concentration (IC_{50}) being 2.1 μM, which is consistent with that (2.4 μM) obtained by the electrochemical biosensor.[56] Moreover, the relative activity of M.SssI MTase decreases when the 5-Aza-dC concentration increases (Figure 4B), with the measured IC_{50} being 1.3 μM, which is in good agreement with that (1.3 μM) measured by a glucometer sensor.[57]

Detection of M.SssI MTase Activity in Serum. To demonstrate the proof of concept of real sample analysis, we measured the recovery ratio of the spiked M.SssI MTase in serum. The recovery ratio is measured to be 98.8−111.5% with an RSD of 1.8−3.8% (Table 1), suggesting the great potential of this PEC biosensor for complex sample analysis.

CONCLUSIONS

We have constructed a new cathodic PEC biosensor to sensitively detect M.SssI MTase using the COP film as the photoactive material. This cathodic PEC biosensor is constructed by the *in situ* growth of p-type COP films onto

https://doi.org/10.1021/acs.analchem.1c01797
Anal. Chem. 2021, 93, 10310−10316

Table 1. Measurement of the Spiked M.SssI MTase in Serum

samples	spiked (U mL^{-1})	detected (U mL^{-1})	RSD (%)	recovery (%)
1	10.0	11.1	2.8	111.5
2	0.5	0.5	3.8	100.2
3	0.1	0.1	1.8	98.8

ITO at room temperature and the subsequent assembly of biotin- and HS-labeled dsDNA probe containing the M.SssI MTase recognition sequence onto the COP film *via* the biotin−streptavidin interaction. The COP thin films possess a porous ultrathin nanosheet structure with abundant active sites, facilitating the generation of a high photocurrent compared with the hydrothermally synthesized ones. The presence of DNA methyltransferases facilitates the introduction of AuNPs to the dsDNA probes *via* the S−Au bond and the intercalation of RhB into the DNA grooves for the production of an enhanced photocurrent. The SPR effect of AuNPs and dye-photosensitized enhancement can significantly amplify the photocurrent of the PEC biosensor. This cathodic PEC biosensor can screen the potential inhibitors and sensitively detect M.SssI MTase in serum as well.

■ ASSOCIATED CONTENT

Supporting Information

The Supporting Information is available free of charge at https://pubs.acs.org/doi/10.1021/acs.analchem.1c01797.

Reagents and materials, apparatus and characterization, photocurrent response of the bulk COP (synthesized by hydrothermal method)-modified ITO electrode and the COP film (*in situ* synthesis)-modified ITO electrode, optimization of experimental conditions, comparison of the proposed PEC biosensor with the reported biosensors for M.SssI MTase assay (PDF)

■ AUTHOR INFORMATION

Corresponding Authors

Xiliang Luo − *Key Laboratory of Optic-Electric Sensing and Analytical Chemistry for Life Science, MOE; Shandong Key Laboratory of Biochemical Analysis; Key Laboratory of Analytical Chemistry for Life Science in Universities of Shandong; and College of Chemistry and Molecular Engineering, Qingdao University of Science and Technology, Qingdao 266042, China;* orcid.org/0000-0001-6075-7089; Phone: +86 0531-86186033; Email: xiliangluo@qust.edu.cn; Fax: +86 0531-82615258

Xiaolei Wang − *College of Chemistry, Chemical Engineering and Materials Science, Collaborative Innovation Center of Functionalized Probes for Chemical Imaging in Universities of Shandong, Key Laboratory of Molecular and Nano Probes, Ministry of Education, Shandong Provincial Key Laboratory of Clean Production of Fine Chemicals, Shandong Normal University, Jinan 250014, China;* orcid.org/0000-0003-1718-8495; Email: wangxl@sdnu.edu.cn

Chun-Yang Zhang − *College of Chemistry, Chemical Engineering and Materials Science, Collaborative Innovation Center of Functionalized Probes for Chemical Imaging in Universities of Shandong, Key Laboratory of Molecular and Nano Probes, Ministry of Education, Shandong Provincial Key Laboratory of Clean Production of Fine Chemicals, Shandong Normal University, Jinan 250014, China;* orcid.org/0000-0002-8010-1981; Email: cyzhang@sdnu.edu.cn

Authors

Lin Cui − *College of Chemistry, Chemical Engineering and Materials Science, Collaborative Innovation Center of Functionalized Probes for Chemical Imaging in Universities of Shandong, Key Laboratory of Molecular and Nano Probes, Ministry of Education, Shandong Provincial Key Laboratory of Clean Production of Fine Chemicals, Shandong Normal University, Jinan 250014, China*

Jingzhu Shen − *College of Chemistry, Chemical Engineering and Materials Science, Collaborative Innovation Center of Functionalized Probes for Chemical Imaging in Universities of Shandong, Key Laboratory of Molecular and Nano Probes, Ministry of Education, Shandong Provincial Key Laboratory of Clean Production of Fine Chemicals, Shandong Normal University, Jinan 250014, China*

Chen-Chen Li − *Key Laboratory of Optic-Electric Sensing and Analytical Chemistry for Life Science, MOE; Shandong Key Laboratory of Biochemical Analysis; Key Laboratory of Analytical Chemistry for Life Science in Universities of Shandong; and College of Chemistry and Molecular Engineering, Qingdao University of Science and Technology, Qingdao 266042, China*

Pei-Pei Cui − *Shandong Provincial Key Laboratory of Biophysics, Shandong Universities Key Laboratory of Functional Biological Resources Utilization and Development, College of Life Science, Dezhou University, Dezhou 253023, China*

Complete contact information is available at: https://pubs.acs.org/10.1021/acs.analchem.1c01797

Author Contributions

‖L.C., J.S., and C.-C.L. contributed equally.

Notes

The authors declare no competing financial interest.

■ ACKNOWLEDGMENTS

This work was supported by the National Natural Science Foundation of China (grant nos. 21735003, 21605096, and 21974080), the Taishan Scholar Program of Shandong Province of China (ts20110829), and the Award for Team Leader Program of Taishan Scholars of Shandong Province, China.

■ REFERENCES

(1) Robertson, K. D. *Nat. Rev. Genet.* **2005**, *6*, 597−610.
(2) Goren, A.; Cedar, H. *Nat. Rev. Mol. Cell Biol.* **2003**, *4*, 25−32.
(3) Bondurant, A. E.; Huang, Z.; Whitaker, R. S.; Simel, L. R.; Berchuck, A.; Murphy, S. K. *Gynecol. Oncol.* **2011**, *123*, 581−587.
(4) Zhang, L.; Zhang, Z.-Y.; Liang, R.-P.; Li, Y.-H.; Qiu, J.-D. *Anal. Chem.* **2014**, *86*, 4423−4430.
(5) Coppieters, N.; Dieriks, B. V.; Lill, C.; Faull, R. L. M.; Curtis, M. A.; Dragunow, M. *Neurobiol. Aging* **2014**, *35*, 1334−1344.
(6) Friso, S.; Choi, S.-W.; Dolnikowski, G. G.; Selhub, J. *Anal. Chem.* **2002**, *74*, 4526−4531.
(7) Chen, F.; Zhao, Y. *Analyst* **2013**, *138*, 284−289.
(8) Cui, L.; Zhao, M.-h.; Li, C.-c.; Wang, Q.; Luo, X.; Zhang, C.-y. *Anal. Chem.* **2021**, *93*, 2974−2981.
(9) Lewin, J.; Schmitt, A. O.; Adorjan, P.; Hildmann, T.; Piepenbrock, C. *Bioinformatics* **2004**, *20*, 3005−3012.
(10) Li, W.; Liu, Z.; Lin, H.; Nie, Z.; Chen, J.; Xu, X.; Yao, S. *Anal. Chem.* **2010**, *82*, 1935−1941.

(11) Ohta, S.; Yamura, K.; Inasawa, S.; Yamaguchi, Y. *Chem. Commun.* **2015**, *51*, 6422−6425.
(12) Tang, R.; Xue, J.; Xu, B.; Shen, D.; Sudlow, G. P.; Achilefu, S. *ACS Nano* **2015**, *9*, 220−230.
(13) Li, J.; Tu, W.; Li, H.; Han, M.; Lan, Y.; Dai, Z.; Bao, J. *Anal. Chem.* **2014**, *86*, 1306−1312.
(14) Li, X.; Zhu, L.; Zhou, Y.; Yin, H.; Ai, S. *Anal. Chem.* **2017**, *89*, 2369−2376.
(15) Li, F.; Wang, S.; Yin, H.; Chen, Y.; Zhou, Y.; Huang, J.; Ai, S. *ACS Sens.* **2020**, *5*, 1092−1101.
(16) Zhou, Y.; Yin, H.; Zhao, W.-W.; Ai, S. *Coord. Chem. Rev.* **2020**, *424*, 213519.
(17) Yin, H.; Sun, B.; Zhou, Y.; Wang, M.; Xu, Z.; Fu, Z.; Ai, S. *Biosens. Bioelectron.* **2014**, *51*, 103−108.
(18) Li, H.; Wang, J.; Wang, X.; Lin, H.; Li, F. *ACS Appl. Mater. Interfaces* **2019**, *11*, 16958−16964.
(19) Meng, L.; Xiao, K.; Zhang, X.; Du, C.; Chen, J. *Biosens. Bioelectron.* **2020**, *150*, 111861.
(20) Lim, S. Y.; Shen, W.; Gao, Z. *Chem. Soc. Rev.* **2015**, *44*, 362−381.
(21) Zhao, W.-W.; Yu, P.-P.; Xu, J.-J.; Chen, H.-Y. *Electrochem. Commun.* **2011**, *13*, 495−497.
(22) Montalti, M.; Cantelli, A.; Battistelli, G. *Chem. Soc. Rev.* **2015**, *44*, 4853−4921.
(23) Liao, X.; Zhang, L.; Wang, S.; Lei, J. *Electrochem. Commun.* **2019**, *100*, 60−63.
(24) Liao, X.; Luo, J.; Wu, J.; Fan, T.; Yao, Y.; Gao, F.; Qian, Y. *Electroanal. Chem.* **2018**, *829*, 129−137.
(25) Victorious, A.; Saha, S.; Pandey, R.; Soleymani, L. *Angew. Chem., Int. Ed.* **2021**, *60*, 7316−7322.
(26) Cui, L.; Hu, J.; Wang, M.; Diao, X.-k.; Li, C.-c.; Zhang, C.-y. *Anal. Chem.* **2018**, *90*, 11478−11485.
(27) Wang, G.-L.; Shu, J.-X.; Dong, Y.-M.; Wu, X.-M.; Zhao, W.-W.; Xu, J.-J.; Chen, H.-Y. *Anal. Chem.* **2015**, *87*, 2892−2900.
(28) Walter, M. G.; Warren, E. L.; Mckone, J. R.; Boettcher, S. W.; Mi, Q.; Santori, E. A.; Lewis, N. S. *Chem. Rev.* **2010**, *110*, 6446−6473.
(29) Yan, K.; Liu, Y.; Yang, Y.; Zhang, J. *Anal. Chem.* **2015**, *87*, 12215−12220.
(30) Zhu, Y.; Yan, K.; Xu, Z.; Wu, J.; Zhang, J. *Biosens. Bioelectron.* **2019**, *131*, 79−87.
(31) Gong, L.; Dai, H.; Zhang, S.; Lin, Y. *Anal. Chem.* **2016**, *88*, 5775−5782.
(32) Cui, L.; Shen, J.; Ai, S.; Wang, X.; Zhang, C.-y. *Biosens. Bioelectron.* **2020**, *168*, 112545.
(33) Udachyan, I.; Kandaiah, S. *J. Phys. Chem. C* **2019**, *123*, 17075−17082.
(34) Tang, J.; Liu, X.; Yang, C.; Zhang, Z.; Sun, R.; Li, H.; Li, C.; Wang, F. *Adv. Mater.* **2019**, *9*, 42533−42542.
(35) Wang, Y.; Cheng, Y.; Wu, N.; Zhang, Z. *ACS Appl. Nano Mater.* **2020**, *3*, 8598−8603.
(36) Gu, X.; Shaw, L.; Gu, K.; Toney, M. F.; Bao, Z. *Nat. Commun.* **2018**, *9*, 534.
(37) Sun, B.; Liu, J.; Cao, A.; Song, W.; Wang, D. *Chem. Commun.* **2017**, *53*, 6303−6306.
(38) Oh, E.; Hong, M.-Y.; Lee, D.; Nam, S.-H.; Yoon, H. C.; Kim, H.-S. *J. Am. Chem. Soc.* **2005**, *127*, 3270−3271.
(39) Zhao, H.; Jin, Z.; Su, H.; Jing, X.; Sun, F.; Zhu, G. *Chem. Commun.* **2011**, *47*, 6389−6391.
(40) Wang, X.; Han, X.; Zhang, J.; Wu, X.; Liu, Y.; Cui, Y. *J. Am. Chem. Soc.* **2016**, *138*, 12332−12335.
(41) Lu, H.; Wang, C.; Chen, J.; Ge, R.; Leng, W.; Dong, B.; Huang, J.; Gao, Y. *Chem. Commun.* **2015**, *51*, 15562−15565.
(42) Mendoza-Cortes, J. L.; Pascal, T. A.; Goddard, W. A. *J. Phys. Chem. A* **2011**, *115*, 13852−13857.
(43) Zhang, C.; Li, C.; Liu, Y.; Zhang, J.; Bao, C.; Liang, S.; Wang, Q.; Yang, Y.; Fu, H.; Wang, K.; Cui, D. *Adv. Funct. Mater.* **2015**, *25*, 1314−1325.
(44) Gomes, R.; Bhaumik, A. *RSC Adv.* **2016**, *6*, 28047−28054.
(45) Bai, L.; Gao, Q.; Zhao, Y. *J. Mater. Chem. A* **2016**, *4*, 14106−14110.
(46) Zhao, W.-W.; Tian, C.-Y.; Xu, J.-J.; Chen, H.-Y. *Chem. Rev.* **2012**, *48*, 895−897.
(47) Li, R.; Yan, R.; Bao, J.; Tu, W.; Dai, Z. *Chem. Commun.* **2016**, *52*, 11799−11802.
(48) Li, J.; Tu, W.; Li, H.; Han, M.; Lan, Y.; Dai, Z.; Bao, J. *Anal. Chem.* **2014**, *86*, 1306−1312.
(49) Peng, B.; Tang, L.; Zeng, G.; Fang, S.; Ouyang, X.; Long, B.; Zhou, Y.; Deng, Y.; Liu, Y.; Wang, J. *Biosens. Bioelectron.* **2018**, *121*, 19−26.
(50) Yan, Z.; Wang, Z.; Miao, Z.; Liu, Y. *Anal. Chem.* **2016**, *88*, 922−929.
(51) Liu, Z.; Zhou, F.; Wu, J.; Yao, Y.; Guo, Y.; Liao, X.; Gao, F.; Qian, Y.; Qian, Y. *J. Electroanal. Chem.* **2018**, *823*, 253−260.
(52) Gadwal, I.; Sheng, G.; Thankamony, R. L.; Liu, Y.; Li, H.; Lai, Z. *ACS Appl. Mater. Interfaces* **2018**, *10*, 12295−12299.
(53) Makula, P.; Pacia, M.; Macyk, W. *J. Phys. Chem. Lett.* **2018**, *9*, 6814−6817.
(54) Li, L.; Duan, L.; Wen, F.; Li, C.; Wang, M.; Hagfeldt, A.; Sun, L. *Chem. Commun.* **2012**, *48*, 988−990.
(55) Kawawaki, T.; Takahashi, Y.; Tatsuma, T. *J. Phys. Chem. C* **2013**, *117*, 5901−5907.
(56) Sui, J.; Wang, L.; Zhao, W.; Hao, J. *Chem. Commun.* **2016**, *52*, 6993−6996.
(57) Chen, Y.; Yi, H.; Xiang, Y.; Yuan, R. *Anal. Chim. Acta* **2018**, *1001*, 18−23.

NOTE ADDED AFTER ASAP PUBLICATION

This paper was published ASAP on July 14, 2021. Changes were made to the y-axis of Figure 4, and the corrected version was reposted on July 15, 2021.

https://doi.org/10.1021/acs.analchem.1c01797
Anal. Chem. 2021, 93, 10310−10316